Research Square

Preprints are preliminary reports that have not undergone peer review.
They should not be considered conclusive, used to inform clinical practice,
or referenced by the media as validated information.

Rapid 3D Printing Method for the Accurate Reproduction of Aortic Aneurysms for clinical trials and educational applications

Elisa Pizzi

elisa.pizzi@unipegaso.it

University of Rome Tor Vergata Faculty of Engineering: Universita degli Studi di Roma Tor Vergata Macroarea di Ingegneria https://orcid.org/0000-0003-4509-2589

Daniele Marazzi

Federica Trovalusci

Research Article

Keywords: aortic aneurysms, Additive Manufacturing Stereolithography (AM SLA), Computed Tomography Angiography (CTA), Endovascular Aneurysm Repair (EVAR), model 3D printing, geometric and optical characterization

Posted Date: July 17th, 2026

DOI: https://doi.org/10.21203/rs.3.rs-10057449/v1

License: This work is licensed under a Creative Commons Attribution 4.0 International License. Read Full License

Abstract

Aortic aneurysm is a severe medical condition characterized by the pathological dilation of the aorta, the main blood vessel in the human body. This study proposes a novel patient specific approach for producing three-dimensional (3D) models of aortic aneurysms using Additive Manufacturing (AM) by AM Stereolithography (AM SLA) 3D printing technology from computed tomography (CT) scans of real cases. A specific elastomer was employed to match the mechanical properties of the biological tissue, particularly endowed with suitable elasticity and flexibility, and relevant for accurate reproduction of the morphology and structure of aortic aneurysms, which is essential for advanced medical applications such as surgical training and preoperative planning. A virtual model generated through CT scans was converted into a physical model using AM SLA technology, ensuring high-fidelity 3D replication. The geometric analysis of the 3D model provides an in-depth understanding of the compliance to the structural and morphological characteristics of real aneurysms, offering accurate data about size, shape, and pathology specifications. In addition, an optical analysis was conducted on the model, by investigating its transparency to the visible light for direct visualization of the internal model's details. The results of this study offer significant contributions to improving diagnostic accuracy and optimizing treatment planning for the treatment of aortic aneurysms. The integration of rapid geometric and optical study with AM SLA 3D printing technology represents an advance in the production of realistic 3D models, enhancing preoperative clinical trials and educational applications and providing new perspectives in the treatment of this clinical condition.

Introduction

An aortic aneurysm is a serious condition that involves the abnormal dilation of the aortic artery. The artery is composed of a series of lamellar elements, including smooth muscle, elastin, collagen, and other tissues that affect its chemical and physical properties [(1),(2)]. During the cardiac cycle, the artery undergoes changes in geometry, with a diameter ranging from 18 to 26 mm during diastole and 19 to 28 mm during systole, and a thickness ranging from 1.2 ± 0.3 to 2.3 ± 0.6 mm [(3)].

The pathogenesis of an aneurysm is attributable to the destruction of the connective tissue in the aortic wall due to the degradation of elastin and the partial involvement of the muscular component, resulting in the accumulation of collagen [(1),(4)]. This process leads to the development of a discontinuity in the stiffness map of the aorta, which fragmentizes the muscle fibers present on the endothelial wall, causing a loss of mechanical properties and the formation of a sac due to the compression and release of the cardiovascular system [(5)]. Several potential contributing factors to this condition include aging, hypertension, atherosclerosis, or genetic predispositions [(6)].

By a clinical point of view, aneurysm necessitates a highly delicate surgical intervention, the rupture of which may result in fatality in as many as 90% of cases [(7)]. It is essential to differentiate between the abdominal segment (AAA) and thoracic segment (TAA) of the aortic artery, which are the two primary areas affected [(8)]. The treatment options available for aneurysm include Endovascular Aneurysm Repair (EVAR) intervention and conventional surgery [(9)]. Studies have shown that the rupture of an aneurysm occurs when the thickness of the artery wall surpasses 1.78 ± 0.22 mm [(10)], while emergency intervention is necessary when the

external diameter of the artery exceeds 5.50 mm and exhibits distensibility [11],[12]. Moreover, it is crucial to consider the angle of the aortic neck, specifically the infra-renal neck angle, as many EVAR implants fail due to excessively high values [13]. Prior to the surgical intervention, diagnostic tests will be conducted to identify the inclination angle of the aneurysm[14].

In recent years, there has been a significant increase in the success rate of EVAR interventions due to the advent of Additive Manufacturing (AM) in the medical field [15]. The success of the intervention is closely associated with the creation of suitable 3D models that accurately and faithfully reproduce the morphology of the anatomical area subject to surgery[16]. These models allow surgeons to assess critical issues during preoperative planning and to test tools to be used during the different phases of surgery treatments. Additionally, the stent can be tested during the preoperative phase to ensure it can be adapted as much as possible to the nonlinear geometry[17].

To create these 3D models, different image acquisition technologies can be used as starting point, such as Computed Tomography (CT) [18] and computed tomography angiography (CTA) [19]. However, the accuracy of the acquired images may be affected by inherent issues related to the resolution of the diagnostic examination machine.

To enhance the efficacy of the intervention, 3D CAD models can be generated from CTA, for instance, in order to facilitate the development of Computational Fluid Dynamic (CFD) simulations using appropriate software analysis. This approach enables the identification of critical issues that may arise both during and after the intervention [20]. Furthermore, the utilisation of the 3D model enables the establishment of a diagnostic process that incorporates a CFD analysis, which subsequently yields the rupture time of the aneurysm under examination [21].

The mechanical properties of the material used is another aspect to be considered for the creation of 3D models [22]. The model can be realised using a variety of materials, although those with flexible properties, such as silicones or elastomers (polyurethanes), are preferred due to their deformability and resilience, which make them suitable for simulating blood vessels [23]. Anyway, the choice among different manufacturing approaches will depend on the type of material to be used. In the case of use of a light-curing elastomer, it is possible to opt for a direct manufacturing method that involves appropriate AM technology for the realization of the final model [24]. By contrast, when the model is realized using silicones, a reverse engineering process is needed. This process begins usually with the realization of 3D moulds by using water-soluble materials, followed by the subsequent coating phase with the silicone material [25]. It is, however, crucial to acknowledge that both production types will present challenges related to the timing of model realization, which will consequently impact the final intervention time on the patient [24],[25].

In this respect, some works employed several mould casting techniques using 3D printing of the mould to realize 3D models of aortic aneurysms applied for numerical simulation in EVAR applications [25],[26]. In these cases, the use of 3D printing to realize silicone moulds for producing models by casting processes conducted to good agreement of the experimental results with finite element analysis (FEA) simulations.

In case of realization of 3D models to be used directly as implantable components, a study about cranial prosthesis [27] evaluated both strengths and limitations of the three main strategies that imply additive manufacturing for the production: (i) direct printing of PLA (polylactic acid) skullcaps, mould casting of poly(methyl methacrylate) (PMMA) prosthesis using (ii) silicone mould manufactured from a 3D printed master, (iii) 3D printed TPU (thermoplastic polyurethane) mould. In that study all solutions adopted led to good geometric accuracy and excellent mechanical resistance of the prosthesis. Direct printing of the PLA resulted in the fastest strategy, followed by PMMA casting in a silicone mould. Anyway, the use of silicone was considered more advantageous overall, due to lower costs and the possibility of achieving sterilization by using autoclaving.

Otherwise, in the case of the creation of 3D models intended mainly for surgical training, the sterilization phase becomes unnecessary, so much so that a direct 3D printing technique, without the use of intermediate steps for the realization of the moulds, should become the technique of choice as the fastest method to shorten the time between training sessions and the final surgical intervention, which represents an extremely crucial element.

Despite the aforementioned issues, models created using AM technology with the most suitable materials are capable of accurately replicating the pre-operative challenges, such as the simulation of cannula insertion into the intended vessel [28].

In order to enhance the probability of success of the intervention, materials with a very low refractive index would be preferred. This will enable the operator to observe the trajectory of the probe/tool and identify any potential issues in the preoperative phase [29].

The objective of this study is to realize a 3D model of an aortic aneurysm at the abdominal aortic aneurysm (AAA) position using direct additive manufacturing (AM) by a stereolithography (SLA) technology. The model realized has been subjected to a preliminary examination of its geometric, mechanical and optical (light transmittance) properties. In particular, the optical transparency of the model has been evaluated by a practical test involving the insertion of a vascular guide into the model, and by determining its visibility. The optical visibility of the inner guide through the model has been evaluated in two modes and compared: 1) taking the model as is in air and 2) submerging it in a liquid to determine change of the refractive index.

Materials and Methods

a) Materials

A Zortrax Inkspire 3D printer (Zortrax, Olsztyn, Poland), based on DLP technology, and a UV light-curing resin (BioMed Elastic 50A, Formlabs, Somerville, MA, USA) especially optimized for traditional SLA 3D printers, were employed to fabricate the model aneurysm. The photopolymer enabled the attainment of a Shore 50A hardness at the conclusion of the manufacturing process, according to the producer's data sheet.

b) Methods

The CTA of the patient (pixel spacing: 0.5 mm × 0.5 mm; slice thickness: 1 mm) was acquired at St. Olavs Hospital (Trondheim, Norway), using a Siemens scanner (Sectra Somatom, Syngo CT) in accordance with a study protocol approved by the regional ethics committee (REK 2016/533, Faculty of Medicine, Trondheim, Norway) [25]. A preliminary STL file was generated from the previously processed DICOM file to elaborate the three-dimensional surface model of the aneurysm formation. The preliminary STL was then processed using appropriate mesh processing software (GeoMagic Design X). At this stage, the acquisition of the model was verified, any defects deriving from the pristine CTA were removed, and the mean thickness of the vessel was estimated, with a theoretical value of 1.00 mm being imposed. A new STL file was generated from this, which was finally processed by a slicing software (ZSuite) for the model production phase. In this phase, the various printing parameters were set, as detailed in Table 1. The positioning of the model was optimized in order to obtain the least number of supports.

Table 1 Printing parameters for slicing software (ZSuite) used to realize the model

Parameter	Value
Layer Thickness	0.05 mm
Exposure Temp	40 s
Off Exposure Temp	5 s
Exposure Time First Layer	120 s
Number of First Layer	6 s
Supplement Time Exposure	No

The printing phase was completed in 2d 1h 41m, by employing approximately 25 ml of resin, as estimated by the slicing software.

The geometrical characterization of the model was performed after the printing phase. Firstly, the thickness of the model's wall was measured in three selected different areas, corresponding to the three external vessels' walls (identified as Input, Output 1 and Output 2) and also to the wall of the central area (Central wall), respectively through a) a digital micrometer directly on the printed physical model, and b) elaboration by CAD software of the photographic image of the printed model. Corresponding to the areas selected, four measurements for each of the selected points (number eight points) were performed, and then the average values and related standard deviations were calculated, both in case of direct measurement (a) that in case of image elaboration (b).

Tortuosity of the arteria affected by aneurysm was also evaluated by CAD elaboration conducted on the image of the printed model. In this case, the axis of revolution of the artery was determined as the curve of the points corresponding to the mean centers of the cross-sections in the printed model. The curve representing the revolution axis was then elaborated by calculating the first and second derivatives to determine the radii of curvature; their variation along the entire curve is related to the longitudinal tortuosity of the reconstructed aneurysm.

The optical transparency of the model was evaluated through the insertion of a vascular guide and subsequent assessment of its optical visibility. The test was conducted by two different methods. By the first, a vascular guide was inserted into the model cavity exposed directly to air. In the second method, the guide was inserted in the model previously immersed in a liquid (an isopropyl alcohol solution) by producing a change in the refractive index [25].

Statistical Analysis

Thickness analysis was performed at eight different points in each model section. Four measurements were acquired for each point, and the mean value was provided with its standard deviation. The curve relative to the central axis of revolution on the model section and the curvature values in the three different concavity change zones were determined graphically using CAD software. All curvature data for the three zones were processed and provided as the mean value and its standard deviation.

Results

Figure 1 shows the graphical elaboration of the model as processed by the Z Suite slicing software, before the printing phase.

The final printed model is represented in the photographic image of Fig. 2. The model was subjected to an initial post-processing phase, during which the weights were compared with those obtained from the slicing process. The model had a weight of 37.15 g, with an initial estimation error of 32.90%. Furthermore, the Shore hardness referred to the A scale was evaluated, resulting in a value of 54.20, which is consistent with the values reported in the material datasheet.

The wall thickness of the 3D model was evaluated with regard to its variability at the vessels' positions designated as Input, Output 1 and Output 2 in Fig. 2, and at the central area (after slicing of the printed model). For accurate measurement of the walls' thickness, the scheme shown in Fig. 3 for the Input, Output 1 and Output 2 positions, was employed, from which the values given in Table 2 of appropriate standard deviation were determined.

Table 2 Comparison of the thickness values by direct measurements through digital micrometer and by image elaboration, referring to the three outer vessels' walls and the central wall of the physical model (8 positions of measurement are depicted in Figure 3, respectively - Values of the average thicknesses calculated from four different measurements are also reported, with relative percentage error respect to the theoretical values from CAD (1 mm).

Position	Thickness [mm]							
	Input wall		**Output 1 wall**		**Output 2 wall**		**Central wall**	
	Direct	From image	Direct	From image	Direct	From image	Direct	From image
1	1.05 ± 0.25	1.18 ± 0.08	0.78 ± 0.09	0.82 ± 0.22	0.66 ± 0.03	0.54 ± 0.03	0.85 ± 0.2	1.58 ± 0.27
2	0.95 ± 0.25	1.45 ± 0.07	0.85 ± 0.04	1.05 ± 0.23	0.63 ± 0.04	0.52 ± 0.02	0.80 ± 0.17	0.86 ± 0.3
3	0.80 ± 0.21	1.35 ± 0.08	0.80 ± 0.07	1.03 ± 0.22	0.43 ± 0.06	0.51 ± 0.03	0.90 ± 0.15	1.05 ± 0.32
4	0.85 ± 0.23	1.4 ± 0.06	0.75 ± 0.03	0.96 ± 0.25	0.45 ± 0.04	0.53 ± 0.04	0.77 ± 0.22	0.88 ± 0.33
5	0.95 ± 0.24	1.15 ± 0.07	0.79 ± 0.03	0.95 ± 0.23	0.54 ± 0.05	0.53 ± 0.04	0.78 ± 0.23	0.75 ± 0.32
6	0.86 ± 0.23	1.13 ± 0.08	0.79 ± 0.04	1.25 ± 0.24	0.46 ± 0.05	0.44 ± 0.05	0.82 ± 0.18	1.02 ± 0.28
7	0.90 ± 0.24	1.35 ± 0.09	0.82 ± 0.05	1.57 ± 0.23	0.50 ± 0.03	0.56 ± 0.03	0.85 ± 0.22	1.21 ± 0.29
8	0.96 ± 0.24	1.25 ± 0.07	0.88 ± 0.03	1.03 ± 0.22	0.56 ± 0.04	0.57 ± 0.03	0.88 ± 0.24	1.09 ± 0.31
Average value	**0.9 ± 0.2**	**1.3 ± 0.1**	**0.8 ± 0.1**	**1.1 ± 0.2**	**0.5 ± 0.1**	**0.53 ± 0.04**	**0.8 ± 0.05**	**1.1 ± 0.3**
Δ error (%)	**-10**	**+30**	**-20**	**+10**	**-50**	**-47**	**-20**	**+10**

Table 2 illustrates also the average thickness values in relation to the four reference areas, with the percentage error calculated in accordance with the theoretical thickness set in the CAD (1 mm).

The values obtained, as they are compared to the theoretical values from the CAD model, indicate that the percentage error in the wall thickness is the greatest for both the testing methods adopted, in the Output 2 area, while it is reduced in the other areas. This could be indicative in some problem arising during the printing phase in that position.

The images in Fig. 4 show a photograph of the vertical section of the aneurysm model (Fig. 4A) with a graphical highlighting of the right and left edges of the section (Fig. 4B). Figure 4C shows the CAD processing of the image acquired on the section, for the determination of the axis of revolution of the artery (referring to its tortuosity).

The figure shows the segments representing the radii of curvature obtained from the derivation of the axis of revolution. As shown in the figure, the change in the concavity of the axis corresponds to the three zones highlighted as blue areas. Table 3 shows the calculated and graphed values of the radii of curvature and their average variation from one zone to another of change in the concavity of the internal axis.

Table 3
Variation of the radii of curvature of the model's central axis (tortuosity parameter) for the three concavity change zones. The average value and related standard deviation are calculated for each zone

Axis point	Calculated radii of curvature [mm]		
	First zone	Second zone	Third zone
1	1.25	3.64	0.65
2	18.02	6.43	1.29
3	35.40	6.18	2.43
4	46.82	5.64	3.72
5	46.08	5.20	5.17
6	41.50	4.50	6.03
7	35.65	3.90	6.97
8	35.01	3.42	-
9	37.25	2.91	-
10	43.92	4.44	-
11	49.34	6.12	-
12	42.94	7.93	-
13	35.52	9.46	-
14	23.98	11.26	-
15	11.76	12.91	-
16	3.59	13.75	-
17	0.94	14.12	-
18	-	13.56	-
19	-	12.30	-
20	-	11.52	-
21	-	11.01	-
22	-	11.03	-
23	-	11.09	-
24	-	11.92	-
25	-	13.31	-

Axis point	Calculated radii of curvature [mm]		
	First zone	Second zone	Third zone
26	-	12.61	-
27	-	10.71	-
28	-	8.62	-
29	-	6.20	-
30	-	3.40	-
31	-	1.88	-
32	-	1.08	-
Average value	**30.00 ± 16.00**	**8.00 ± 4.00**	**4.00 ± 2.00**

An investigation was conducted to determine the effectiveness of inserting the vascular guide into the model (Fig. 5). During the initial test, in which the model was exposed to air, the process of inserting the vascular guide proved to be more challenging than in the second method, where the model was submerged in a fluid, isopropyl alcohol (Fig. 6). The presence of the fluid made it easier for the tool to pass through, significantly reducing the difficulty of insertion. This disparity can be attributed to the friction generated between the tool and the walls of the model, which is greater in air and impedes the optimal performance of the instrument. In the second mode, with the model submerged in isopropyl alcohol, the friction is significantly reduced, making it easier to insert the vascular guide.

The evaluation of optical transparency was carried out on the model in accordance with the procedures outlined. In the first scenario, where the vascular guide was introduced into the model in contact with air, there was a reduction in transparency resulting from the refraction of light on the surfaces, which made the vascular guide less eye-visible and, consequently, less handy (Fig. 4).

In the second mode, the model's immersion in the liquid phase led to a substantial increase in transparency. This improvement can be ascribed to the favourable difference in the refractive index from the presence of a surrounding liquid, which diminishes internal refractions and light scattering. The decrease in the air-solid interface enables greater light penetration and transmission through the model, thereby enhancing the visibility of the vascular guide inserted within it (Fig. 5). Consequently, a clearer and more defined visualization of the internal structures is achieved, which facilitates the observation by the operator and meticulous internal analysis of the structure.

Conclusions

In this study, a three-dimensional model of an aortic aneurysm in an abdominal aortic aneurysm (AAA) position was analyzed and developed. After conducting a preliminary phase during which the DICOM file from the computed tomography (CT) scan was studied and an STL file was generated, the production phase by 3D printing of the model was performed. During production phase, the printing parameters were

configured to produce the physical model, which was subsequently subjected to geometric characterization and evaluation of optical characteristics in terms of transparency and external visibility of the operating tools. The geometric analysis of the thicknesses was conducted in different areas (external and central), allowing for a non-destructive evaluation in case of the external areas and a destructive one in case of the central area. Geometric variations of the thickness from the theoretical model, was determined both by direct measurement through digital micrometer and photographic image CAD elaboration. The measurements then allowed for the determination of the average thickness and standard deviation, making possible to highlight discrepancies due to random errors, method errors, and errors due to the printing process. The analysis of this data on the printed model constitutes a preliminary assessment set useful to the surgeon in order to further facilitate and speed up the following operational training phase. Moreover, the optical feasibility tests showed that when the model was exposed to air, the refraction of light on the surface reduced the transparency of the model, making it difficult to view the vascular guide clearly by the operator. However, the immersion of the model in a liquid phase with refractive index similar to the model's material, allowed for a clearer and more defined visibility of the vascular guide tool. These findings demonstrate that immersion in a liquid is a more effective method for carrying out operability training. In conclusion, 3D printing in this field has been used so far mainly to realize moulds intended for the direct casting of models used in clinical trials. The method involved, by the direct 3D printing of a model from computed tomography (CT) scans, enables a fast patient-specific approach aimed at enhancing clinical trials and educational sessions and providing new practical perspectives in the treatment of this clinical condition.

Declarations

Funding

The authors received no financial support for the research, authorship, and/or publication of this article.

Competing Interests

The authors declare that they have no known competing financial interests or personal relationships that could have appeared to influence the work reported in this paper.

Availability of Data and Materials

Data sets generated during the current study are available from the corresponding author on reasonable request.

References

1. He CM, Roach MR. The composition and mechanical properties of abdominal aortic aneurysms. J Vasc Surg. 1994;20:6–13.
2. Laurent S, Boutouyrie P, Lacolley P. Structural and Genetic Bases of Arterial Stiffness. Hypertension. 2005;45:1050–5.

3. Arko FR, Murphy EH, Davis CM, Johnson ED, Smith ST, Zarins CK. Dynamic geometry and wall thickness of the aortic neck of abdominal aortic aneurysms with intravascular ultrasonography. J Vasc Surg. 2007;46:891–7.
4. Forte A, Della Corte A, De Feo M, Cerasuolo F, Cipollaro M. Role of myofibroblasts in vascular remodelling: focus on restenosis and aneurysm. Cardiovasc Res. 2010;88:395–405.
5. Li Z, Pei M, Zhang J, Liu N, Wang J, Zou D. A study to characterize the mechanical properties and material constitution of adult descending thoracic aorta based on uniaxial tensile test and digital image correlation. Front Bioeng Biotechnol. 2023;11.
6. Haque K, Bhargava P. Abdominal Aortic Aneurysm [Internet]. 2022. Available from: www.aafp.org/afp
7. Karthikesalingam A, Holt PJ, Vidal-Diez A, Ozdemir BA, Poloniecki JD, Hinchliffe RJ, Thompson MM. Mortality from ruptured abdominal aortic aneurysms: clinical lessons from a comparison of outcomes in England and the USA. The Lancet. 2014;383:963–9.
8. Ehrman JK, Fernandez AB, Myers J, Oh P, Thompson PD, Keteyian SJ. Aortic Aneurysm. J Cardiopulm Rehabil Prev. 2020;40:215–23.
9. Verhoeven ELG, Vourliotakis G, Bos WTGJ, Tielliu IFJ, Zeebregts CJ, Prins TR, Bracale UM, van den Dungen JJAM. Fenestrated Stent Grafting for Short-necked and Juxtarenal Abdominal Aortic Aneurysm: An 8-Year Single-centre Experience. European Journal of Vascular and Endovascular Surgery. 2010;39:529–36.
10. Zhai Y, Delgado AI, Sameti M, Dong P, Xiong W, Bashur CA, Gu L. Biomechanical Characterization of Abdominal Aortic Aneurysm: The Rupture Mechanism. Applied Sciences. 2024;14:613.
11. Satriano A, Rivolo S, Martufi G, Finol EA, Di Martino ES. In vivo strain assessment of the abdominal aortic aneurysm. J Biomech. 2015;48:354–60.
12. van ‘t Veer M, Buth J, Merkx M, Tonino P, van den Bosch H, Pijls N, van de Vosse F. Biomechanical properties of abdominal aortic aneurysms assessed by simultaneously measured pressure and volume changes in humans. J Vasc Surg. 2008;48:1401–7.
13. Schanzer A, Greenberg RK, Hevelone N, Robinson WP, Eslami MH, Goldberg RJ, Messina L. Predictors of Abdominal Aortic Aneurysm Sac Enlargement After Endovascular Repair. Circulation. 2011;123:2848–55.
14. Rockley M, Hadziomerovic A, van Walraven C, Bose P, Scallan O, Jetty P. A new “angle” on aortic neck angulation measurement. J Vasc Surg. 2019;70:756-761.e1.
15. He Z, Mongrain R, Lessard S, Chayer B, Cloutier G, Soulez G. Anthropomorphic and biomechanical mockup for abdominal aortic aneurysm. Med Eng Phys. 2020;77:60–8.
16. Biglino G, Capelli C, Wray J, Schievano S, Leaver L-K, Khambadkone S, Giardini A, Derrick G, Jones A, Taylor AM. 3D-manufactured patient-specific models of congenital heart defects for communication in clinical practice: feasibility and acceptability. BMJ Open. 2015;5:e007165.
17. Branzan D, Geisler A, Grunert R, Steiner S, Bausback Y, Gockel I, Scheinert D, Schmidt A. The Influence of 3D Printed Aortic Models on the Evolution of Physician Modified Stent Grafts for the Urgent Treatment of Thoraco-abdominal and Pararenal Aortic Pathologies. European Journal of Vascular and Endovascular Surgery. 2021;61:407–12.

18. Bartolozzi C, Neri E, Caramella D. CT in vascular pathologies. Eur Radiol. 1998;8:679–84.
19. Törnqvist P, Dias N V, Resch T. Optimizing imaging for aortic repair. J Cardiovasc Surg (Torino). 2015;56:189–95.
20. Polanczyk A, Podyma M, Stefanczyk L, Szubert W, Zbicinski I. A 3D model of thrombus formation in a stent-graft after implantation in the abdominal aorta. J Biomech. 2015;48:425–31.
21. Al-Jumaily AM, Embong AH Bin, AL-Rawi M, Mahadevan G, Sugita S. Aneurysm Rupture Prediction Based on Strain Energy-CFD Modelling. Bioengineering. 2023;10:1231.
22. Guarnera D, Carrera E, Hansen CJ, Maiarù M. Mechanical characterization of 3D printed mimic of human artery affected by atherosclerotic plaque through numerical and experimental methods. Biomech Model Mechanobiol. 2021;20:1969–80.
23. Cornejo J, Cornejo-Aguilar JA, Vargas M, Helguero CG, Milanezi de Andrade R, Torres-Montoya S, Asensio-Salazar J, Rivero Calle A, Martínez Santos J, Damon A, Quiñones-Hinojosa A, Quintero-Consuegra MD, Umaña JP, Gallo-Bernal S, Briceño M, Tripodi P, Sebastian R, Perales-Villarroel P, De la Cruz-Ku G, Mckenzie T, Arruarana VS, Ji J, Zuluaga L, Haehn DA, Paoli A, Villa JC, Martinez R, Gonzalez C, Grossmann RJ, Escalona G, Cinelli I, Russomano T. Anatomical Engineering and 3D Printing for Surgery and Medical Devices: International Review and Future Exponential Innovations. Biomed Res Int. 2022;2022.
24. Ngo TD, Kashani A, Imbalzano G, Nguyen KTQ, Hui D. Additive manufacturing (3D printing): A review of materials, methods, applications and challenges. Compos B Eng. 2018;143:172–96.
25. Emendi M, Støverud KH, Tangen GA, Ulsaker H, Manstad-H F, Di Giovanni P, Dahl SK, Langø T, Prot V. Prediction of guidewire-induced aortic deformations during EVAR: a finite element and in vitro study. Front Physiol. 2023;14.
26. Emendi M, Tangen GA, Di Giovanni P, Ulsaker H, Brekken R, Manstad-Hulaas F, Prot V, Bel-Brunon A, Støverud KH. Aortic roadmapping during EVAR: a combined FEM–EM tracking feasibility study. Int J Comput Assist Radiol Surg. 2024;19:2239–47.
27. Flora B, Scerrati A, Trovalusci F, Vesco S. Patient-specific cranioplasty, by direct and indirect additive manufacturing of biopolymers and implantable materials. The International Journal of Medical Robotics and Computer Assisted Surgery. 2023;19.
28. Coles-Black J, Bolton D, Chuen J. Accessing 3D Printed Vascular Phantoms for Procedural Simulation. Front Surg. 2021;7.
29. Kaufmann R, Zech CJ, Takes M, Brantner P, Thieringer F, Deutschmann M, Hergan K, Scharinger B, Hecht S, Rezar R, Wernly B, Meissnitzer M. Vascular 3D Printing with a Novel Biological Tissue Mimicking Resin for Patient-Specific Procedure Simulations in Interventional Radiology: a Feasibility Study. J Digit Imaging. 2022;35:9–20.

Figures

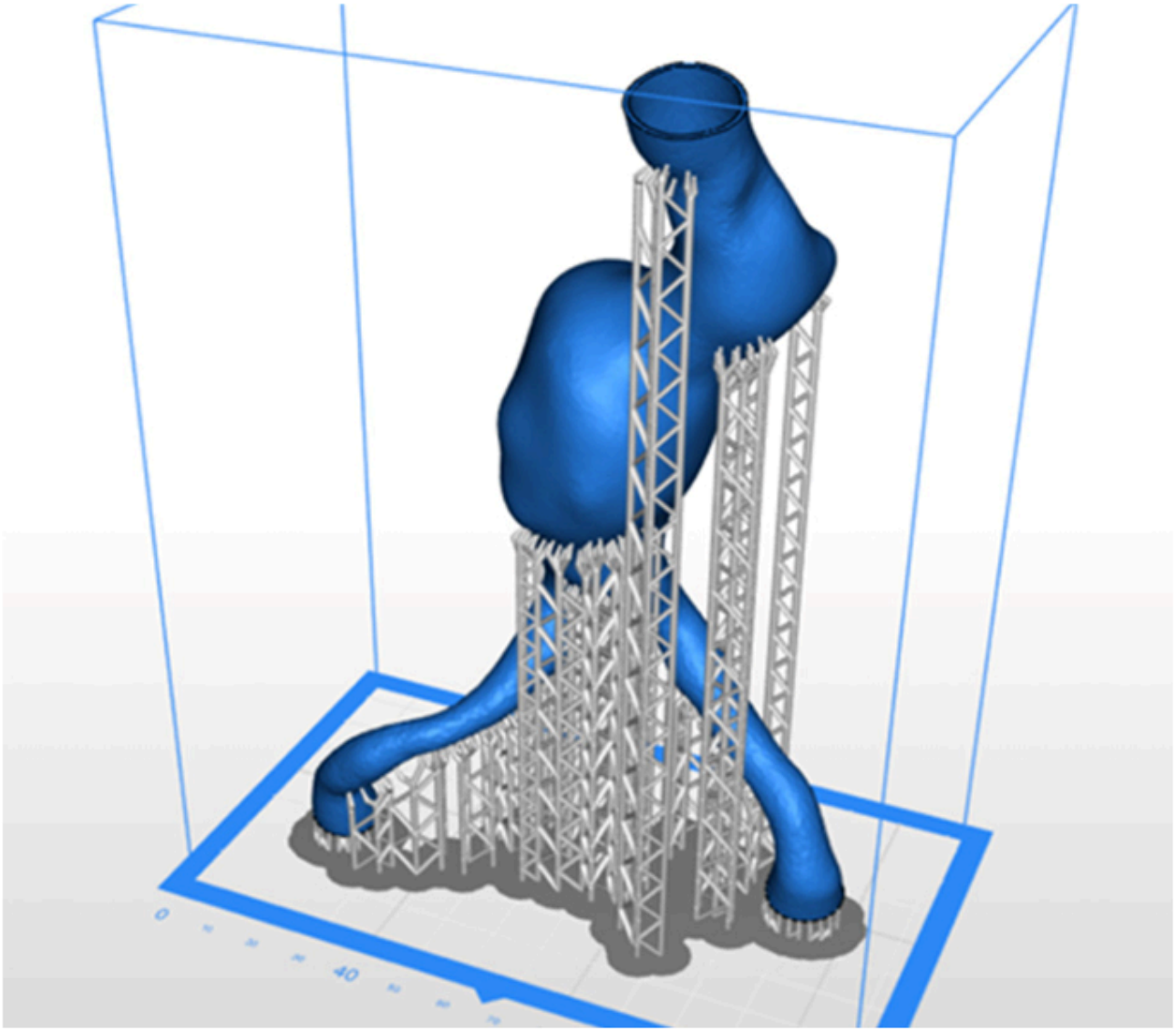


Figure 1

Model of the aneurysm processed by the ZSuite software

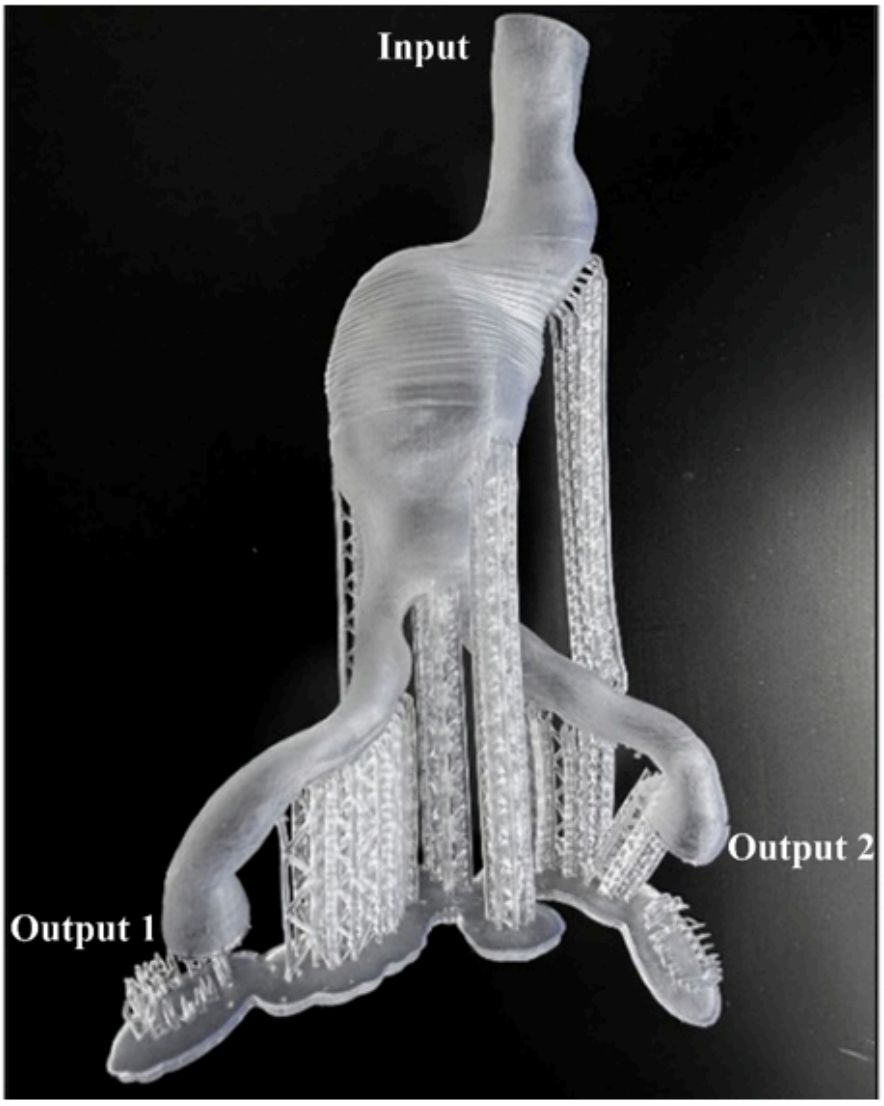


Figure 2

Physical model obtained at the end of the production process. The three sections subjected to geometric analysis of the thickness, referred to as Input, Output 1 and Output 2, are highlighted.

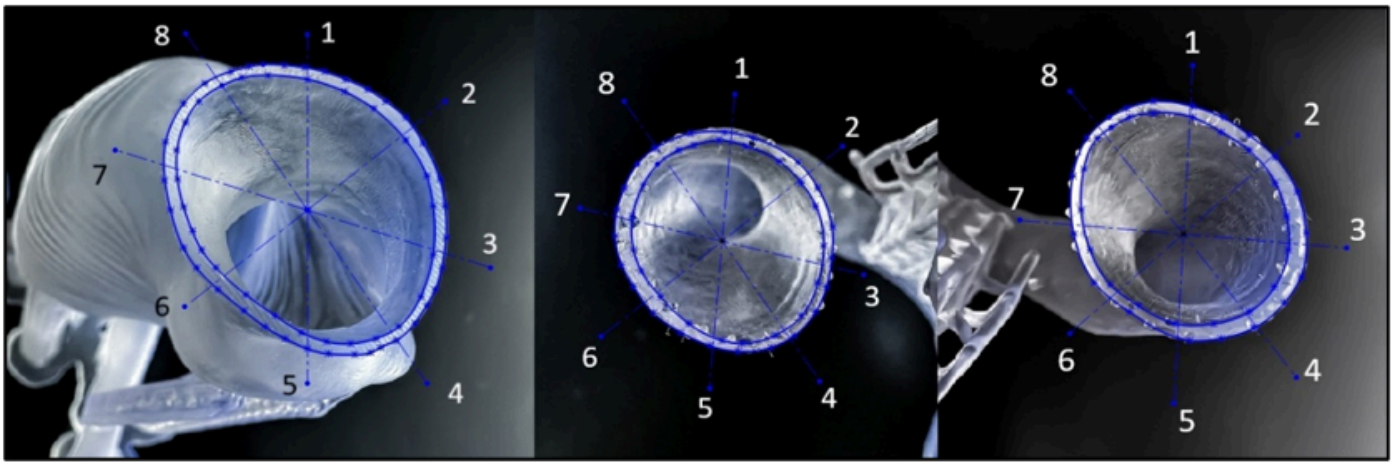


Figure 3

Measurement schemes adopted for the analysis of thicknesses referred to the Input (A), Output 1 (B) and Output 2 (C) sections.

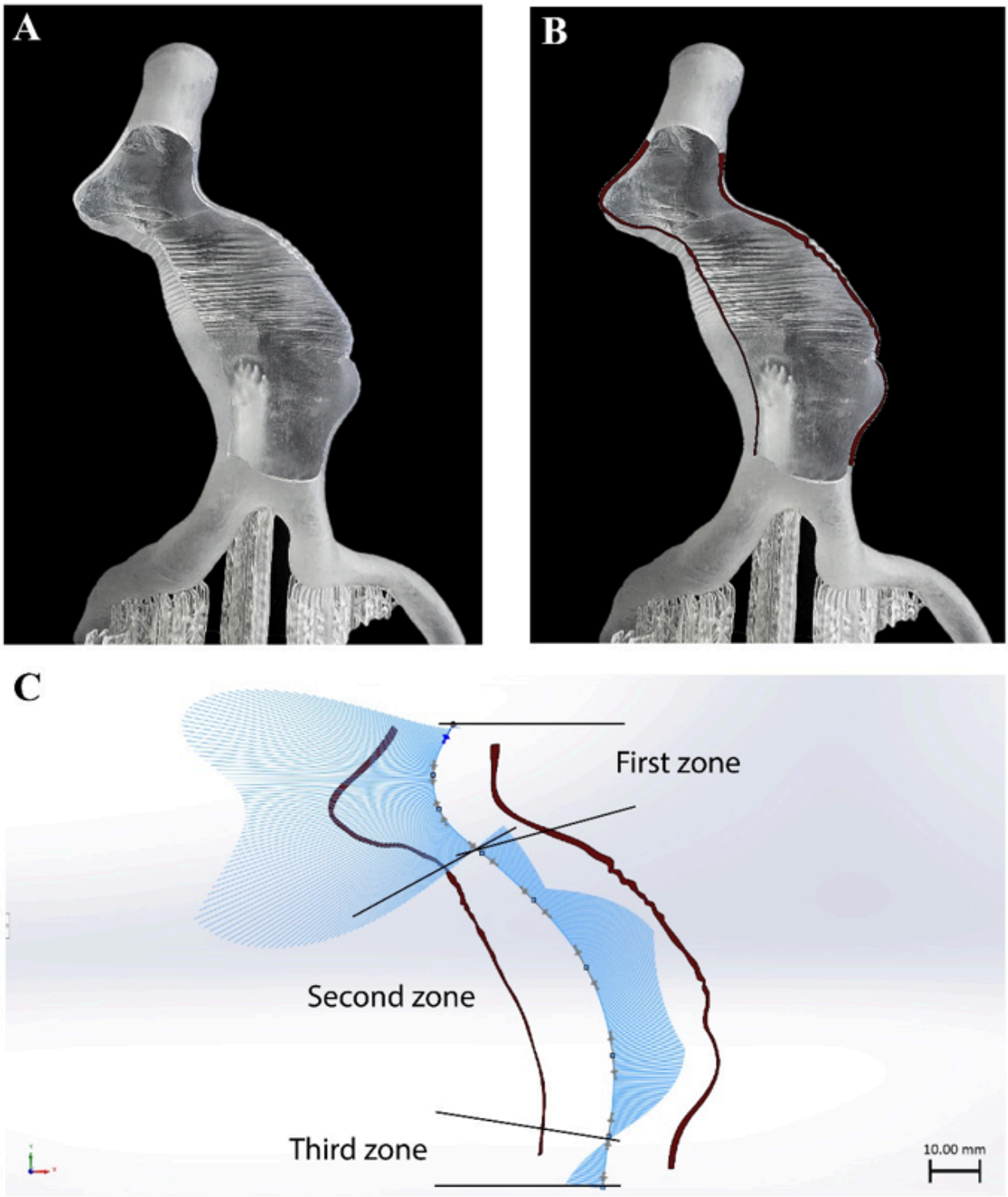


Figure 4

CAD elaboration of the internal section of the model for the determination of the revolution axis and its radii of curvature (tortuosity parameter)



Figure 5

3D model of Aortic Aneurysm during the first test mode (in air) to evaluate optical visibility of inner operating tool



Figure 6

3D model of aortic aneurysm during the second test mode (in liquid, isopropyl alcohol) to evaluate optical visibility of inner operating tool

Supplementary Files

This is a list of supplementary files associated with this preprint. Click to download.

- GraphicalabstractJPEG.jpg